

# A Study on the Grooving Process of a Cross-scored Rupture Disc

Jae Young Jeong<sup>1,2</sup>, Jayone Lee<sup>2</sup>, Sanghoon Yeom<sup>2</sup>, Woongchul Choi<sup>3</sup>,  
Tae Gu Kim<sup>4</sup>, Seung Cheol Hong<sup>4</sup>, Mira Ryu<sup>5</sup>, Heungseob Kim<sup>6</sup> and Seong Beom Lee<sup>6,#</sup>

<sup>1</sup> LHE Co. Ltd., Jangbang-ri, Hanrim-myun, Gimhae, South Korea, 621-874

<sup>2</sup> Department of Mechanical Engineering, Inje University, Eobang-dong, Gimhae, South Korea, 621-749

<sup>3</sup> Graduate School of Automotive Engineering, Kookmin University, Jeongneung-ro 77, Seongbuk-gu, Seoul, South Korea, 136-702

<sup>4</sup> Department of Occupational Health and Safety Engineering, Inje University, Eobang-dong, Gimhae, South Korea, 621-749

<sup>5</sup> BK21 Advanced Vehicle Core Parts Research Group, Inje University, Eobang-dong, Gimhae, South Korea, 621-749

<sup>6</sup> Dept. of Mechanical and Automotive Engineering, High Safety Vehicle Core Technology Research Center, Inje University, Eobang-dong, Gimhae, South Korea, 621-749

# Corresponding Author / E-mail: mechlsb@inje.ac.kr, TEL: +82-55-320-3667, FAX: +82-55-324-1723

KEYWORDS: Rupture disc, Pressure-relief device, Grooving process, Finite element analysis

*High-pressure facilities such as pressure vessels and storage equipment are widely used in all areas of manufacturing. Although many safety regulations have been enacted, mechanical defects and system operator errors sometimes cause industrial disasters. Since industrial disasters at high-pressure facilities cause greater loss of life and property, the installation of pressure-relief devices is mandatory. A rupture disc (also known as a bursting disc) is a type of non-reclosing pressure-relief device, equipped with a leak-tight seal. It is designed to prevent disasters and damage to equipment by immediate, complete rupture when the internal pressure of the plumbing reaches a predetermined level. Various types of rupture discs are cross-scored, and are activated by the reversal of a dome shape and pressure load. They are designed with an X-shaped groove on their surfaces to facilitate bursting without fragmentation. In this research, the processing characteristics of the grooving process, one of the major processes in the production of a cross-scored rupture disc, are investigated via experiments and finite element analysis (FEA) to obtain a design basis for cross-scored rupture discs required by high-pressure facilities with varying kinds of performance. The mechanical properties and chemical composition of the stainless steel used to produce cross-scored rupture discs are determined with a tensile testing machine and an electron microscope. The characteristics of the grooving process are then measured and compared with FEA results.*

Manuscript received: May 20, 2011 / Accepted: August 9, 2011

## 1. Introduction

Many industrial manufacturing facilities, such as chemical plants, petrochemical plants, and pharmaceutical plants, have equipment and piping systems that operate under high temperatures and pressures. There are many hazards that can lead to accidental conflagrations, explosions, and leaks. The hazard factors include ignition problems, excessive overpressure, corrosion, thermal radiation, fatigue, leakage, abrasion, reaction congestion, and technical hitches. In particular, industrial disasters due to excessive overpressure cause equipment and/or piping failures, economic losses to businesses, environmental contamination, and health and safety risks. To reduce the likelihood of such events, equipment and piping systems that operate under high temperatures and pressures must be protected from excessive overpressure. For this reason, pressure-relief devices are installed in industrial manufacturing

facilities.

The use of rupture discs, one type of pressure-relief device, is prescribed by many standards (ASME, AISI, API, DIN, BS, KS, etc.) and by the international organization for standardization (ISO). Standards that apply to rupture discs include the American Society of Mechanical Engineers (ASME) Boiler and Pressure Vessel Code, Section VIII, Division 1; the American Petroleum Institute (API) Recommended Practice 520; and the CE Pressure Equipment Directive 97/23/00. An ASME code-compliant rupture disc carries the UD code symbol. The ISO standards that apply to rupture discs include ISO 4126, ISO 4126-2, and ISO 6718.<sup>1</sup> The rupture disc specifications used in Korea are KS B 6260, KS B ISO 6718, KS B ISO 4162-2, and KS B ISO 4126-6.

A rupture disc, which isolates pressure-relief valves from harmful process media (gas/liquid) and protects against fugitive emissions, is a thin metal disc designed to burst at a specified

pressure. It separates the process fluid from the safety relief valve, and thereby prevents leakage through the valve. Rupture discs have a concave shape and open at a reproducible pressure. They are made of an alloy of stainless steel, Inconel, Monel, aluminum, and nickel. The discs are manufactured with a number of cuts and holes to induce them to burst into regular pieces. On account of these characteristics, rupture disc processing must be sophisticated enough to satisfy installation and operation requirements.

The purpose of this paper is to study the manufacturing characteristics of rupture discs that are cross-scored with an X-shaped pattern on their surfaces to facilitate opening without knife blades. The rupture discs used in this research are limited by type, size, and material. The type is cross-scored. The size is 3 1/2 inches. The material is 316L-grade stainless steel. Standard tensile tests for 316L-grade stainless steel are performed by Instron 8801 test equipment. The results include most of the forms of behavior commonly observed and the strength-related properties of principal interest, and the results are applied to finite element analysis for the simulation of the grooving process of the rupture disc. The processing parameters for the grooving process include the thin-plate thickness and the V-type stamping forces. The experimental processing is carried out using the Instron 8801 test equipment to measure the V-type stamping forces making the grooving shape for each specimen. After the process, the groove depth is measured for each specimen. Finite element analyses are conducted using the general-purpose finite element analysis software ANSYS to estimate the grooving processing of the rupture disc. The analysis results are compared with experimental process results.

## 2. Research Trends

International research on rupture discs includes the work of Friedel on the relationship between the pressure drop of a rupture disc/safety valve unit and the disc charge reduction coefficients for the flow resistance of the safety valve.<sup>2</sup> Tanaka et al. studied the behavior of bursting pressure for rupture discs using two different methods.<sup>3</sup> Chung et al. researched the progressive conceptual design of pressure relief systems for safe processing plants.<sup>4</sup> Köper and Westphal analyzed pressure relief devices located in several major chemical plants.<sup>5</sup> In Korea, Kang experimentally investigated a theoretical model for the forming pressure of a rupture disc.<sup>6</sup>

However, the general research on rupture discs is only focused on the performance evaluation and various types of pressure-relief system. Thus, in this study the grooving process for the cross-scored rupture disc is carried out and compared with finite element analysis results.

## 3. Material Property Tests

The grooving process leads to elastic and plastic deformations of thin-plate stainless steel. Thus, tension tests were conducted on specimens of SUS 316L (or AISI 316L) stainless steel having an

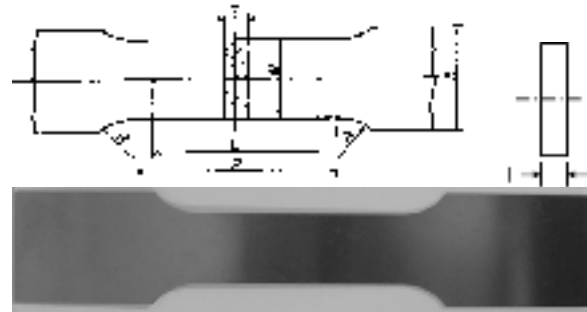


Fig. 1 Standard tensile test specimen: KS B 08018 No. 5, flat, original size



Fig. 2 Tensile test specimen setup with the Instron 8801 test machine

initial length of 17 mm, a wide length of 12.5 mm, a gauge length of 50 mm, and thicknesses of 0.3, 0.4, 0.5, and 0.6 mm. Each thickness of thin-plate made of SUS 316L stainless steel is calculated as below.<sup>7</sup>

$$t_i = \frac{Pb \times k \times d_0}{UTS} \quad i = 0.3, 0.4, 0.5, 0.6$$

where  $Pb$  is a burst pressure ( $0.689\text{N/mm}^2$ ),  $k$  is a factor (each 2.189, 2.919, 3.648, 4.378 for each 0.3, 0.4, 0.5, 0.6 mm of specimen thicknesses),  $d_0$  is required effective discharge diameter (84.7mm), and UTS means ultimate tensile strength ( $426.1\text{N/mm}^2$  at burst temperature,  $260^\circ\text{C}$ ).

A typical specimen is shown in Fig. 1. The tests began with a machined specimen held at both ends by the grips of the tensile test equipment, as shown in Fig. 2. Regarding standard tensile test, the Korean Standard provides that cross-head speed should be assigned within a range of 1.5 to 7 mm per minute. Accordingly, for the tensile test of SUS 316L stainless steel, cross-head speed of 2 mm per minute was selected.

The outputs of the tensile tests were the force-displacement curves shown in Fig. 3. The engineering stress-strain curve obtained from the force-displacement data is shown in Fig. 4. Analysis of the force-displacement curves allowed the yield strengths, elastic (Young's) modulus, uniform strain, and total strain for SUS 316L stainless steel to be determined.

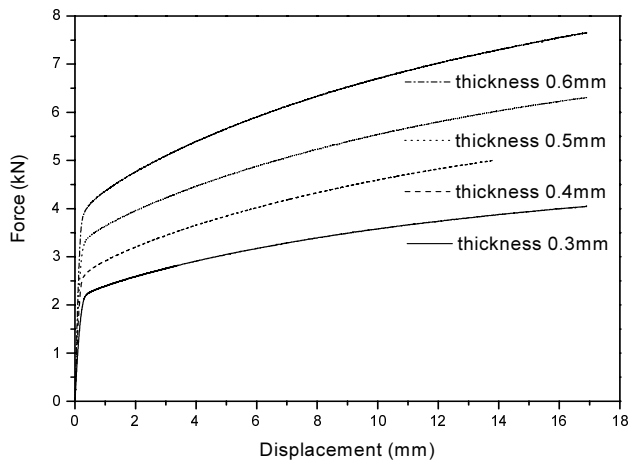


Fig. 3 Force-displacement curve for tensile tests on SUS 316L stainless steel specimens with groove thicknesses of 0.3, 0.4, 0.5, and 0.6 mm

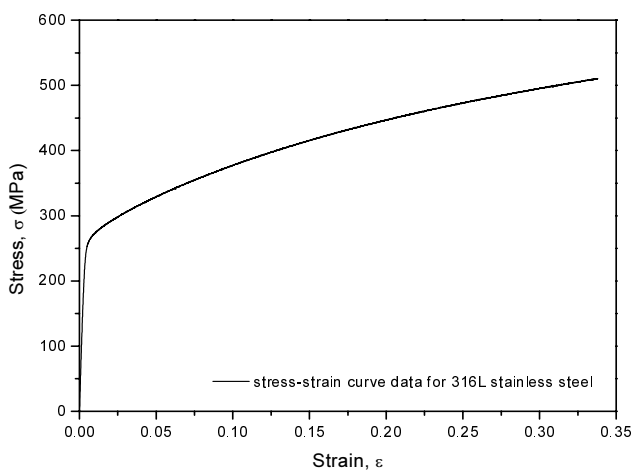


Fig. 4 Engineering stress-strain curve for SUS 316L stainless steel

#### 4. Experiments: Grooving Process Tests

The primary objective of the experimental grooving process tests was to create X-shaped grooves on the surfaces of round thin-plate specimens with various thicknesses.

##### 4.1 Experimental device

To carry out the grooving process experiment, experimental devices were needed. The materials used in the process were chosen to satisfy the required mechanical and physical properties. Except for experimental device, Groove knife, the material was AISI 1045 (JIS S45C), a medium carbon steel with 0.45% carbon content, which provides greater strength and hardness than other types of steel. AISI D2 (JIS G 4404), a high-carbon, high-chromium tool steel alloyed with molybdenum and vanadium, was used for experimental device, Groove knife. The manufactured experimental device parts are shown in Fig. 5. Disc holder fastened the Round thin-plate specimen with Disc holder assembled by 4 of M8 bolt. Groove support is located in Disc holder inside. The assembly consists of Disc holder, Disc holder cover, Groove support, Round

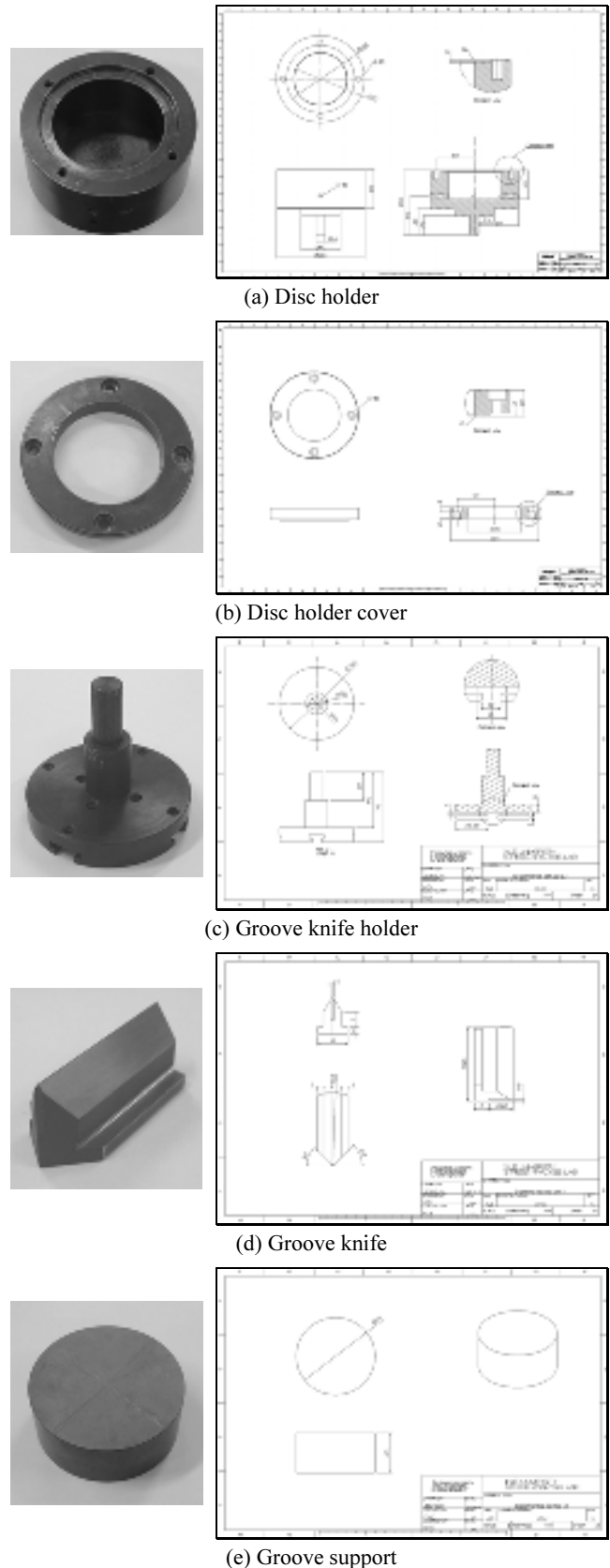


Fig. 5 Experimental device parts

thin-plate specimen is set on the bottom of test machine, INSTRON 8801. Groove knife holder is assembled with Groove knife and is set on the top of test machine. Round test specimens with various thicknesses are shown in Fig. 6.

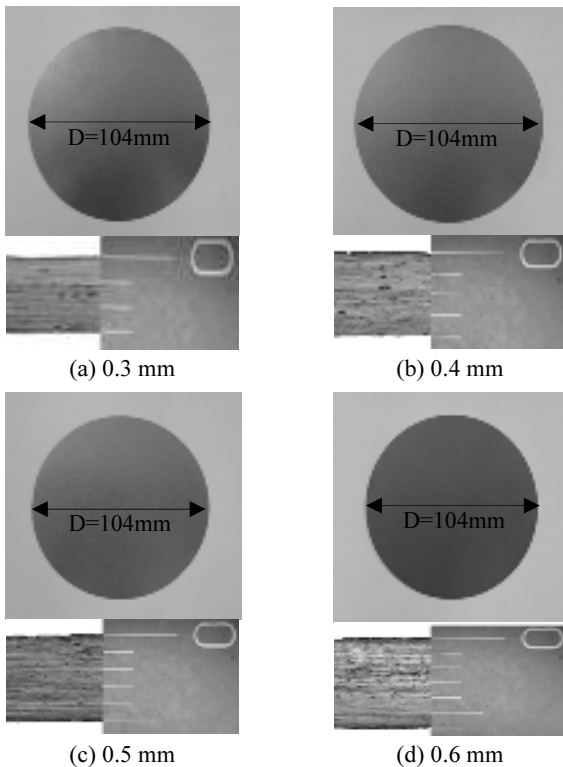


Fig. 6 Round thin-plate specimens: thickness

**4.2 Equipment and setup**

This test was performed using an Instron 8801 servo-hydraulic test machine, which consists of a computer unit, a load frame, a control panel, a controller, and a hydraulic power unit (see Fig. 7). The experimental devices used in this test included five parts: compression devices (Groove knife holder, Groove knife) and holding and support devices (Disc holder, Disc holder cover, Groove support). The components were assembled between Disc holder and Disc holder cover, which were loosely bolted together. The test specimen was also placed between experimental device, Disc holder and Disc holder cover. Groove support was inserted into Disc holder, and functioned as rigid body. Groove knife was situated on top of the test specimen. The parts assembly placed in the test machine is shown in Fig. 8.

**4.3 Implementation**

The V-type stamping deformation and force on the surface of a test specimen cannot be directly measured due to the contact between the compression devices and the surface. Accordingly, the deformation on the surface of each specimen was measured as the difference in the distances of the compression devices. The deformation process was terminated when the compression devices reached a predetermined force, in order to ensure that the stamping deformation on the surface of the test specimen would be measured at this predetermined force (since both the deformation and the force required to deform the plate would then be measured). The cross-head speed associated with the parts assembly and test specimen was 2.5 mm per minute. Tests with slow deformation velocity were carried out at the same speed as the other tests. In their initial state, the compression device and test specimen were



Fig. 7 Test equipment for the grooving process: Instron 8801

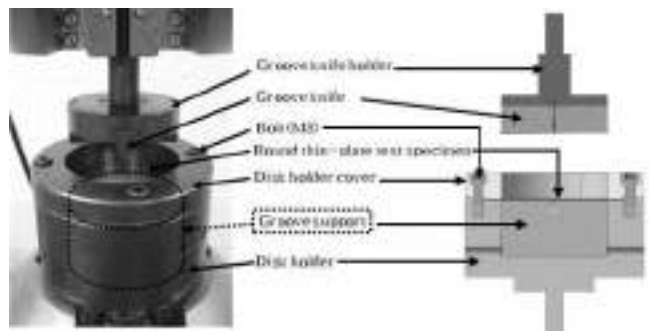


Fig. 8 Parts assembled in the test machine for the grooving process

Table 1 Test conditions for the grooving process

Specimen thickness (mm)	Predetermined forces (kN)			
	0.3	20	30	40
0.4	30	40	50	60
0.5	45	55	65	75
0.6	50	60	70	80

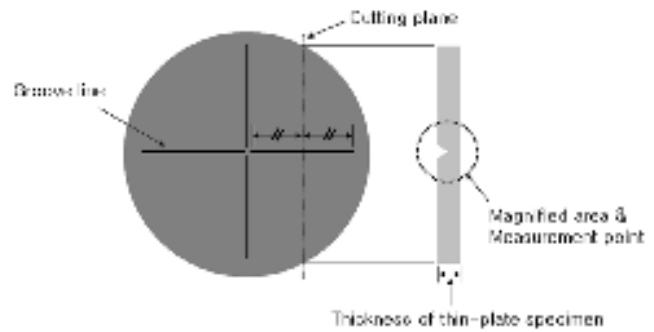


Fig. 9 Cutting plane of a specimen for the grooving process test

just touching, without any deformation of the compression device. The test conditions for the grooving process are listed in Table 1.

**4.4 Results**

Force and displacement were measured in each test. As the parts assembly moved upward toward the compression device, the reaction force and displacement of the compression device were measured by the load cell. After the specimens were cut as shown in Fig. 9, the grooving depths on their surfaces were observed and measured using an optical microscope. The results are shown in Figs. 10-13.

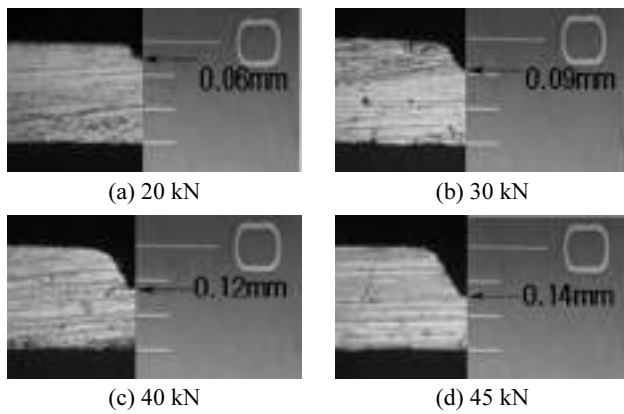


Fig. 10 Grooving depth, thickness 0.3 mm

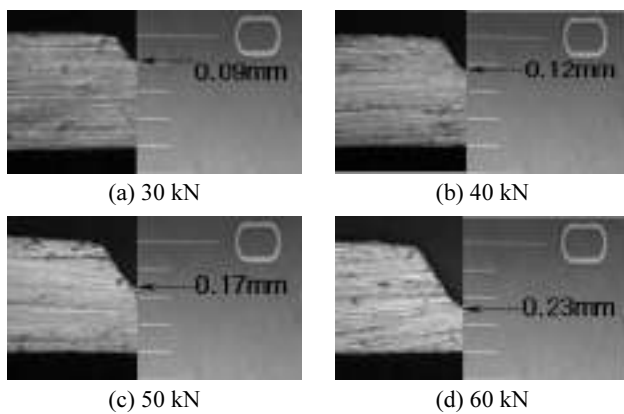


Fig. 11 Grooving depth, thickness 0.4 mm

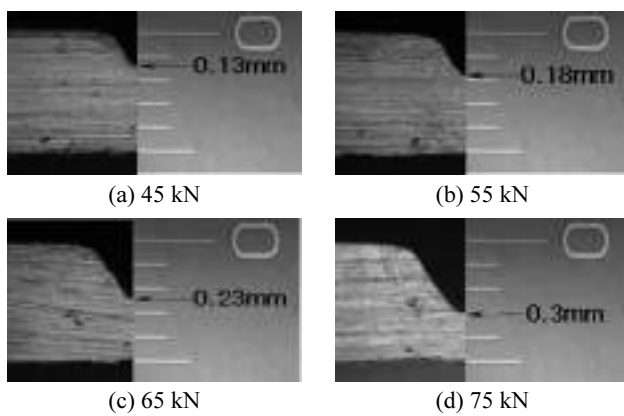


Fig. 12 Grooving depth, thickness 0.5 mm

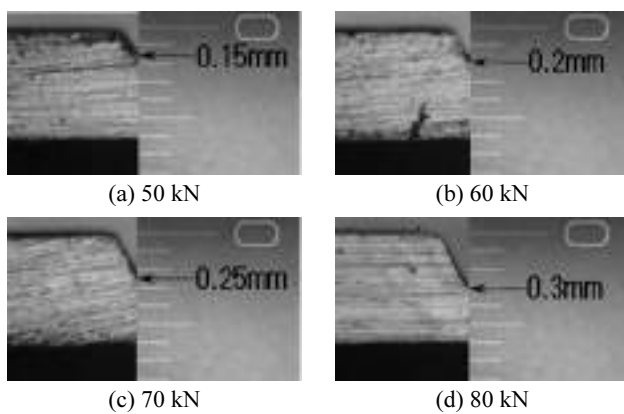


Fig. 13 Grooving depth, thickness 0.6 mm

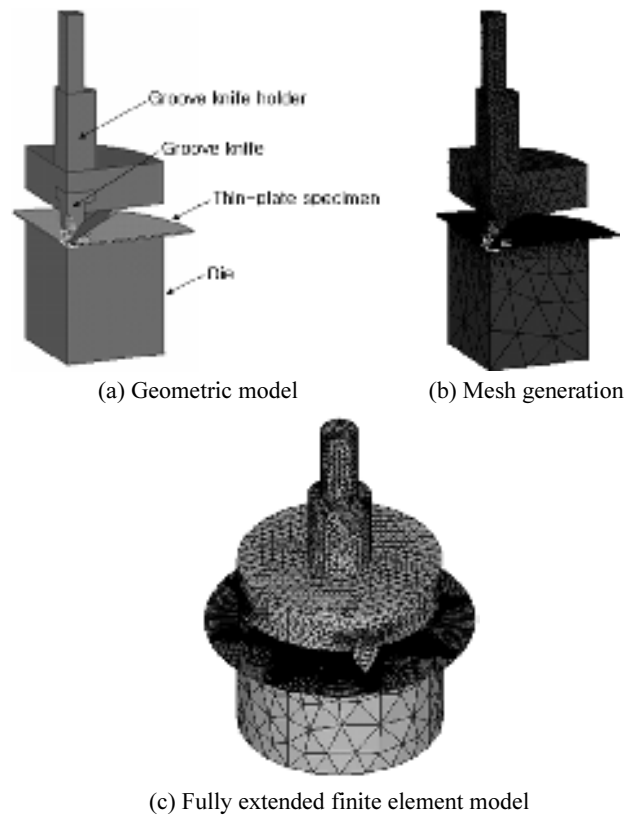


Fig. 14 Computational model for FE analysis of the grooving process

Table 2 Design parameter for the thin-plate model used in the FE analysis of the grooving process

Parameter	Thin-plate model (mm)			
Thickness	0.3	0.4	0.5	0.6

## 5. Finite Element Analysis: Structural Analysis of the Grooving Process

In this section, a finite element analysis of the grooving process is discussed. The purpose of this analysis was to determine the relationship between the displacement of the test jig and the deformation of a thin-plate specimen during the grooving process. All associated computations were performed using the general-purpose finite element analysis software ANSYS.

### 5.1 Geometric model and mesh

The proposed geometric and computational model was described by symmetric extension of the 1/4 model shown in Fig. 14. The geometric model was equal in size to the experimental devices and specimens. The design parameter used in the analysis was the thickness of the specimen (see Table 2).

Two different kinds of elements were used in the ANSYS computational model.<sup>9</sup> The Solid 185 element was used for the thin-plate specimen, and the Solid 45 element was used for the experimental devices. The expected area of contact between the two bodies was represented by a fine mesh near those regions. The finite element modeling information is given in Table 3.

Table 3 Number of nodes and elements used in the FE analysis of the grooving process

	Number of nodes	Number of elements
Thin-plate specimen	18,828	9,246
Groove knife holder	2,579	10,401
Groove knife	2,078	8,190
Groove support	2,333	8,396
Total	25,818	36,230

## 5.2 Boundary conditions

The boundary conditions were designed to avoid rigid body motion, and also to take advantage of the symmetry of the model. Note that in a plane of symmetry, the displacement in the direction perpendicular to the plane must be equal to zero. There are two planes of symmetry in the models shown in Fig. 14. Thus, we required only the one-fourth model of the actual members, as shown in Fig. 14(b). Accordingly, the computational model for structural analysis of the grooving process used nodes placed along both the vertical and horizontal planes of symmetry. The nodes in the bottom area of the model of experimental device, Groove support were constrained to zero displacement in all directions, whereas the models of the upper experimental device parts were movable in the vertical direction to allow for the deformation of the thin-plate model.

## 5.3 Contact

The contact condition between the two bodies was one of the uncertainties in the computational model. However, application of precise contact conditions is essential for obtaining accurate analysis results, and is especially important for rubber-like materials exhibiting large deformations, according to Jang et al. (2011).<sup>10</sup> To model a contact problem, we must first identify the parts to be analyzed and their possible interactions. If one of the interactions is at a point, the corresponding component of the model is a node. If one of the interactions is at a surface, the corresponding component of the model is a beam, shell, or solid element. A finite element model recognizes possible contact pairs by the presence of specific contact elements. These contact elements are overlaid on the parts of the model that are being analyzed for interaction. ANSYS supports four contact models: node-to-node, node-to-surface, surface-to-surface, and beam-to-beam. Each type of model uses a different set of ANSYS contact elements, and is appropriate for a specific type of problem.

In the present analysis, the contact area between the two bodies was treated as flexible-to-flexible. The contact model applied in this analysis was surface-to-surface, which uses a target surface and a contact surface to form a contact pair. The contact element applied in this simulation was Conta174, which is applicable to 3D structural and coupled-field contact analysis. The target element applied in this simulation was Targe 170, which is used to present various 3D target surfaces for the associated contact element Conta 174. The physical connection between the models of experimental device, Groove knife and Groove support was bonded; we assumed that there was no separation and that the two models were always bonded together. For this reason, an internal multipoint constraint

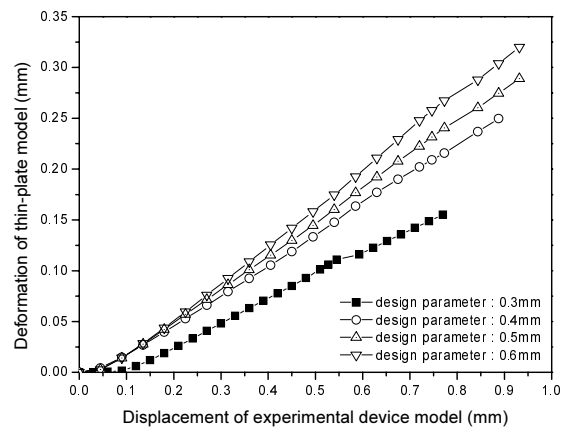


Fig. 15 Displacement-deformation data for the FE analysis of the grooving process with the given design parameter

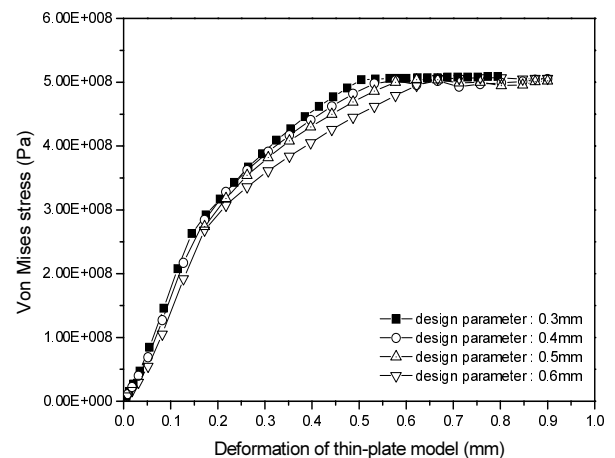


Fig. 16 Von Mises stress-deformation data for the FE analysis of the grooving process with the given design parameter

(MPC) contact algorithm was applied to the contact area between the bodies. However, the connection between the experimental device, Groove knife and thin-plate specimen models required that the target element penetrate the contact element to some extent. The connection between the specimen model and the experimental device, Groove support model was required to also satisfy the same condition. To accomplish this, a penalty function was included in the contact algorithm.

## 5.4 Load

In this analysis, the load was applied as a downward displacement of the upper experimental device models. The displacement began with the upper experimental device models above the surface of the thin-plate specimen model, and ended at 1.25 to 1.5 times the value of the design parameter for the round thin-plate model.

## 5.5 Results

Fig. 15 shows the predicted relationship between the displacement of the experimental device, Groove knife holder model and the deformation of the round thin-plate specimen model. Fig. 16 shows the predicted relationship between the deformation of

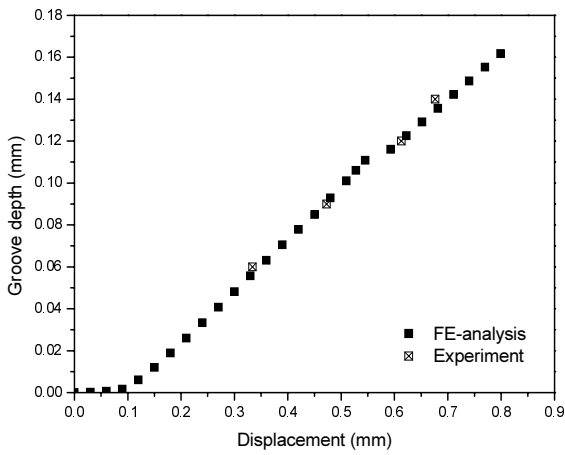


Fig. 17 Comparison of the FE analysis and experimental results for the grooving process for a groove thickness of 0.3 mm

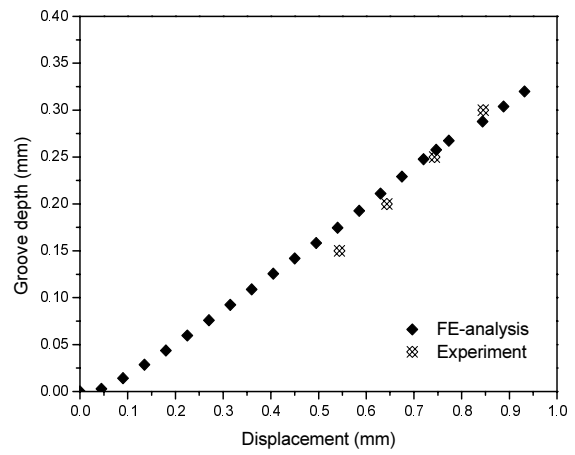


Fig. 20 Comparison of the FE analysis and experimental results for the grooving process for a groove thickness of 0.6 mm

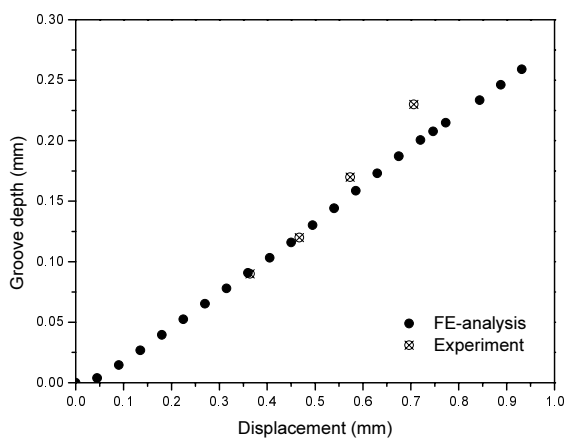


Fig. 18 Comparison of the FE analysis and experimental results for the grooving process for a groove thickness of 0.4 mm

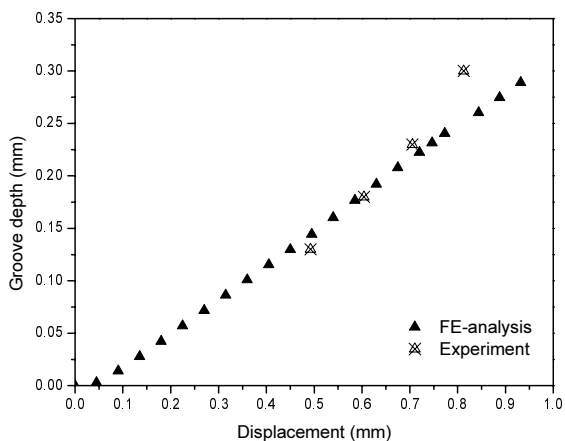


Fig. 19 Comparison of the FE analysis and experimental results for the grooving process for a groove thickness of 0.5 mm

the specimen model and the von Mises stress at the deformation. In the experimental device displacement region from zero to 0.1 mm, the deformation of the thin-plate model did not appear to increase for a design parameter value of 0.3 mm. However, for the other values of the design parameter, increasing deformation could be clearly observed in the same region. For experimental device

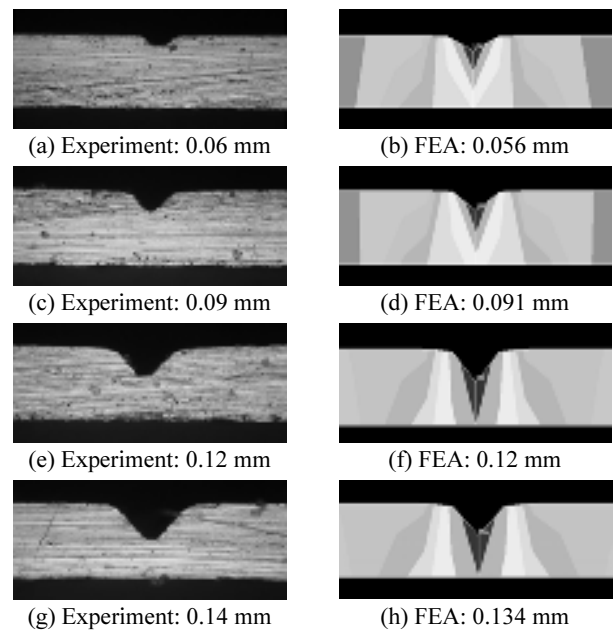


Fig. 21 Comparison of the deformed shapes from the FE analysis and experiment for a groove thickness of 0.3 mm

displacements greater than 0.1 mm, the rate of increase of the deformation of the thin-plate model was nearly linear. For each value of the design parameter, the von Mises stress results were less than the ultimate strength for the material properties under maximum deformation.

## 6. Comparison of FE Analysis and Experimental Results

The FE analysis results were compared to the experimental test results for the grooving process. The experimental data are shown with the FE analysis plots in Figs. 17-20, and the deformed experimental shapes are compared with the FE analysis predictions in Figs. 21-24. In these comparisons, the measurement points covered half of the contact area between the experimental device and the thin-plate specimen. The comparisons were based on the measurement technique used in the experiments.

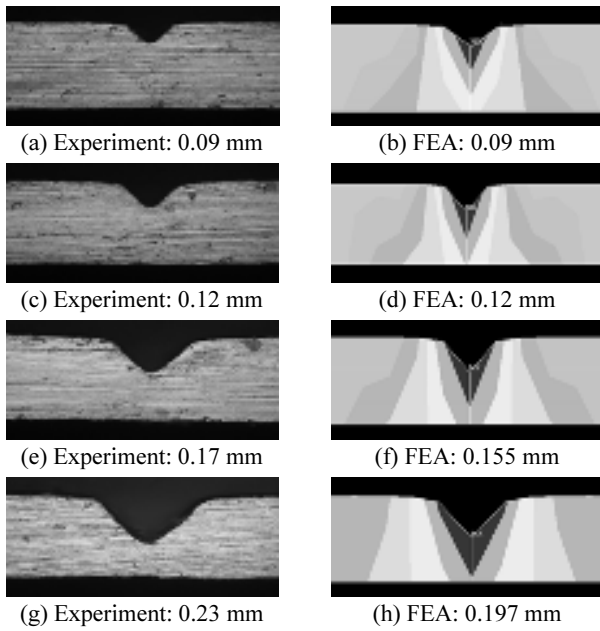


Fig. 22 Comparison of the deformed shapes from the FE analysis and experiment for a groove thickness of 0.4 mm

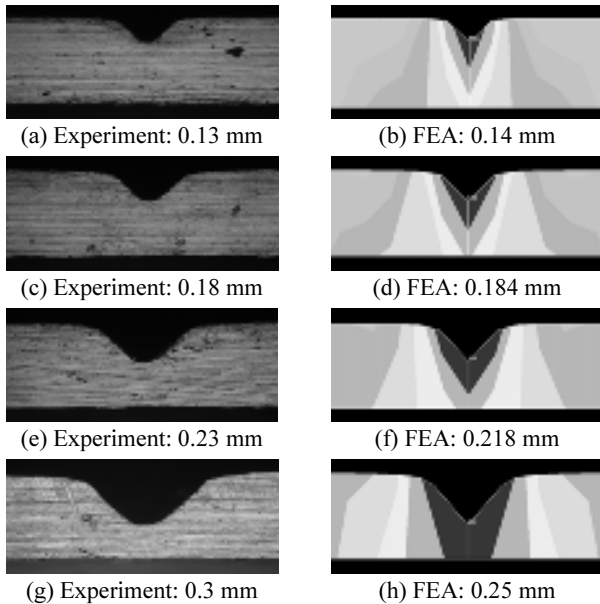


Fig. 23 Comparison of the deformed shapes from the FE analysis and experiment for a groove thickness of 0.5 mm

## 7. Summary and Conclusions

A metal-forming process for manufacturing a scored rupture disc was carried out experimentally, and the experimental results were systematically compared to finite element analysis predictions. The material properties of AISI 316L stainless steel were quantitatively analyzed via an experimental apparatus. The experimental devices used to process the scored rupture disc were designed and manufactured. The FEA-predicted grooving depths for each thin-plate thickness agreed quite well with the experimental results, with a relative error range of less than 20.0 percent. Thus, through the results of this research, it is possible to

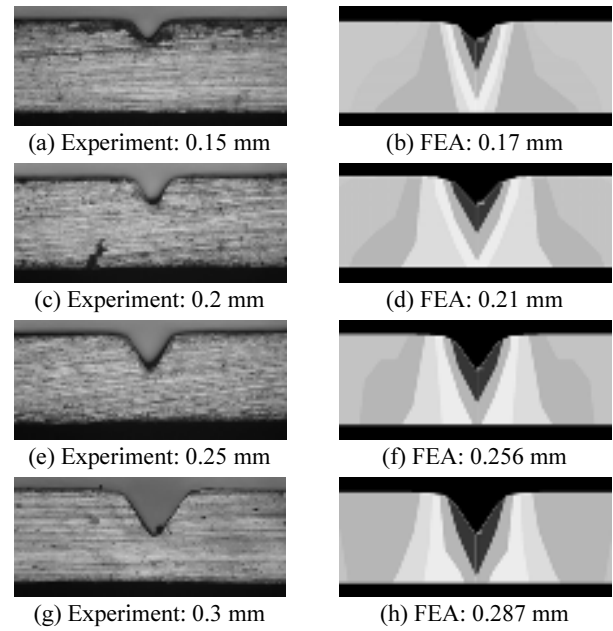


Fig. 24 Comparison of the deformed shapes from the FE analysis and experiment for a groove thickness of 0.6 mm

predict process results via finite element analysis (FEA) prior to actual process of a cross-scored rupture disc.

## ACKNOWLEDGEMENT

This work was supported by grant from Inje University, 2010.

## REFERENCES

- Short, W. E., "Fire versus non-fire contingencies: A study of pressure-relief device sizing risks," *Journal of Pressure Vessel Technology*, Vol. 128, No. 1, pp. 122-129, 2006.
- Friedel, L., "Two phase pressure drop in a rupture disc/safety valve unit," *Journal of Loss Prevention in the Process Industries*, Vol. 1, No. 1, pp. 31-38, 1988.
- Tanaka, N., Wada, Y., Tamura, M. and Yoshida, T., "Performance of pressure vessel test concerned with heating rate of pressure vessel and bursting pressure of rupture disc," *Journal of Hazardous Materials*, Vol. 23, No. 1, pp. 89-107, 1990.
- Chung, P. W. H., Yanga, S. H. and He, C. H., "Conceptual design of pressure relief systems," *Journal of Loss Prevention in the Process Industries*, Vol. 13, No. 6, pp. 519-526, 2000.
- Köper, O. and Westphal, F., "Database-supported documentation and verification of pressure relief device design in chemical plants," *Journal of Loss Prevention in the Process Industries*, Vol. 16, No. 1, pp. 73-79, 2003.
- Kang, Y. K., "Analysis of forming pressure and burst pressure of rupture disc," *Journal of the KSPE*, Vol. 18, No. 6, pp. 109-113, 2001.

7. Lake, G. F. and Inglis, N. P., "The Design and Manufacture of Bursting Discs," Proc. of the Institution of Mechanical Engineers, Vol. 142, No. 1, pp. 365-378, 1939.
8. KS B 0801, "Test Pieces for Tensile Test for Metallic Materials," 1981.
9. ANSYS Inc., "Theory Reference Manual Ver. 10.0," 2009.
10. Jang, W. J., Lee, J., Woo, C. S., Kim, B. K. and Lee, S. B., "An experimental study and finite element analysis of weatherstrip," Int. J. Precis. Eng. Manuf., Vol. 12, No. 1, pp. 97-104, 2011.